High rate cycling performance of lanthanum-modified $Li_4Ti_5O_{12}$ anode materials for lithium-ion batteries

Ting-Feng Yi [a],[*], Ying Xie [b],[**], Qiuju Wu [a],[d], Haiping Liu [c],[***], Lijuan Jiang [a], Mingfu Ye [a], Rongsun Zhu [a]

[a] School of Chemistry and Chemical Engineering, Anhui University of Technology, Maanshan, Anhui 243002, PR China
[b] Key Laboratory of Functional Inorganic Material Chemistry (Heilongjiang University), Ministry of Education, Heilongjiang University, Harbin 150080, PR China
[c] School of Marine Science and Technology, Harbin Institute of Technology, Weihai 264209, PR China
[d] Key Laboratory of Soft Chemistry and Functional Materials, Ministry of Education, Nanjing University of Science and Technology, Nanjing, Jiangsu 210094, PR China

HIGHLIGHTS

► The over-discharge performance of La-modified $Li_4Ti_5O_{12}$ anode is first reported.
► La modification improves the conductivity and reversibility of the $Li_4Ti_5O_{12}$.
► La-modified $Li_4Ti_5O_{12}$ anodes remarkably exhibit high rate performance.

ARTICLE INFO

ABSTRACT

A micro-sized particle $Li_4Ti_{5-x}La_xO_{12}$ ($0 \leq x \leq 0.2$) material has been synthesized by a simple solid-state method at air. The obtained $Li_4Ti_{5-x}La_xO_{12}$ materials are $Li_{3x}La_{2/3-x}TiO_3$ (LLTO)–$Li_4Ti_5O_{12}$ (LTO) solid solution, and well crystallized with a particle size in the range of 1–2 μm. The electronic conductivity and lithium diffusion coefficient of La-modified LTO ($Li_4Ti_{4.95}La_{0.05}O_{12}$) are improved because LLTO exhibits a high ionic conductivity during Li^+ extraction. $Li_4Ti_{4.95}La_{0.05}O_{12}$ material shows discharge capacities of more than 206 and 197 mAh g^{-1} after 100 cycles at 1 C and 3 C charge–discharge rates, respectively. Especially, in rate performance, the $Li_4Ti_{5-x}La_xO_{12}$ ($x = 0.1, 0.2$) samples maintain capacity of about 181 mAh g^{-1} until 5 C rates after 200 cycles, while the pure LTO sample shows a severe capacity decline at corresponding rate. These results suggest that La modifying is an effective way to improve the chemical stability of the electrode in contact with the electrolyte and improve their cyclability and rate capability during long term cycling. Since high rate performance is an important factor that needs to be considered in fabricating power batteries in industry, the La-modified LTO moves closer to real and large-scale applications.

1. Introduction

Rechargeable lithium batteries (LIBs) are widely used in portable equipment today. However, there have always been safety issues arising from their organic electrolytes or electrode materials. These issues are becoming more serious with the increasing size of batteries for use in electric vehicles (EVs), hybrid electric vehicles (HEVs) or load-leveling applications [1,2]. Developing anode materials with high safety is one of the key challenges for lithium-ion batteries. One of the key safety issues in anode for LIBs would be the dendritic lithium growth on the anode surface at high charging current because the conventional carbonous materials approach almost 0 V versus Li/Li^+ at the end of Li insertion [3]. Spinel $Li_4Ti_5O_{12}$ (LTO) has been viewed as one promising alternative to graphite due to its small dimensional change during charge–discharge process and high insertion potential of 1.55 V, which can avoid the reduction of electrolyte on the surface of electrode. However, the poor electronic conductivity of $Li_4Ti_5O_{12}$ limits the sufficient use for high current applications before any materials modifications. The conductivity and rate performance of LTO has been improved by coating with carbon or a metallic conducting layer [4], by doping with metal ions (such as Zn^{2+} [5], Mg^{2+} [6], Ni^{3+} [7], Al^{3+} [8], Cr^{3+} [9], Co^{3+} [9], La^{3+} [10,11], Ga^{3+} [12], Zr^{4+}

[13], Mo^{4+} [14], Ru^{4+} [15], V^{5+} [16,17], Nb^{5+} [18,19], Ta^{5+} [20]) or non-metal ions (F^- [21] and Br^- [22]) in Li, Ti or O sites, or reducing the particle size. Lithium-ion battery has a risk of explosion from possible inner short circuit due to the drastic operational fault conditions, such as over-charge, over-discharge, or short circuits. An internal short is much more dangerous than an external short circuit, because the former induces an enormous heat instantaneously and locally to cause thermal runaway of the electrolyte and electrode materials [23]. High energy density can be obtained either by high voltage or high capacity. Therefore, it is necessary to study the over-discharge behaviors (down to 0 V) of $Li_4Ti_5O_{12}$ anode materials considering the safety and energy density. Although safety and excellent cyclability are contributed to the commercial success of $Li_4Ti_5O_{12}$ and future applications as anode material of power sources (like HEV, EV), power sources also require a high charge–discharge rate capability. Hence, when the electrochemical performances of different anode materials are compared, loading is very important especially at high C rates. Although Gao et al. [10,11] reported the electrochemical performance of lanthanum-doped $Li_4Ti_5O_{12}$ prepared by an outer gel method. It is difficult to meet the commercial applications on lithium-ion batteries due to the complicated synthetic routes and high synthetic cost of sol–gel method mentioned above. From a commercial viewpoint, the solid-state synthesis of LTO material exhibits a potential commercial application due to the simple synthesis route and low synthesis cost. In addition, Gao et al. [10,11] only reported the electrochemical performance between 1 and 3 V, and the charge–discharge rate was not more than 2 C. To our knowledge, no investigation was reported on the rate cycling performance of lanthanum-modified $Li_4Ti_5O_{12}$ ($Li_4Ti_{5-x}La_xO_{12}$) discharged to 0 V synthesized by the solid-state method. In the present work, we reported the rate cycling performance of $Li_4Ti_{5-x}La_xO_{12}$ compound ($0 \le x \le 0.2$) prepared by the solid-state method. A careful investigation has been carried out to give new insights into the structural properties, rate performance, over-discharge performance (down to 0 V) and the modifying effect on the conductivity of the material.

2. Experimental

2.1. Material preparation

La-modified and pure lithium titanates, $Li_4Ti_{5-x}La_xO_{12}$ ($x = 0$, 0.05, 0.1, 0.15, 0.2) were synthesized by a solid-state reaction. TiO_2, Li_2CO_3, and $La(NO_3)_3 \cdot 6H_2O$, used as raw materials, were mixed by ball milling for 4 h in an acetone slurry, followed by drying at 80 °C for 12 h. Finally, the powders were calcined at 850 °C for 24 h in a flowing air atmosphere to obtain the samples. Excessive Li (5 wt%) was provided to compensate for the volatilization of Li during synthesis.

2.2. Material characterization

Thermogravimetry-differential scanning calorimetric analysis (TG–DSC) was performed using a NETZSCH STA 449C in the range of 25–830 °C at a heating rate of 5 °C min^{-1} under flowing air atmosphere. Powder X-ray diffraction (XRD) employing Cu $K\alpha_1$ ($10° < 2\theta < 80°$) radiation was used to identify the crystalline phase of the prepared powders. Raman measurements were performed on a SPEX-1403 Raman spectrometer. The laser light source was the 488 nm line of an Ar^+ laser excited at 400 mW. All the powder samples were pressed into pellets before measurements. A Hitachi S-4000 scanning electron microscope (SEM) was used for morphological studies. Cyclic voltammetry was carried out using a two-electrode system on a CHI 852C electrochemical working station (CH Instrumental) between 0 and 3 V (versus Li/Li^+) at a scanning rate of 0.2 mV s^{-1}. EIS measurements were carried out in two-electrode cells by using Zahner Zennium IM6ex electrochemical workstation with a ±5 mV ac signal and a frequency range from 10^4 to 0.01 Hz. The electrochemical performances of the LTO materials were evaluated using a battery test system, LAND CT2001A model (Wuhan Jinnuo Electronics Co., Ltd.), and the cells were tested at 0.5, 1, 3 and 5 C charge–discharge rate between 0.0 and 2.5 V (versus Li/Li^+), respectively.

2.3. Battery preparation

To evaluate electrochemical performance, composite electrodes were constructed by mixing the $Li_4Ti_{5-x}La_xO_{12}$ ($x = 0$, 0.05, 0.1, 0.15, 0.2), polyvinylidene fluoride (PVDF) dissolved in N-methylpyrolline and carbon black, in the weight ratios 82:10:8. The mixture was prepared as a slurry and spread onto copper foil using the doctor blade technique. Following evaporation of the solvent and drying, electrodes were incorporated into an electrochemical cell (coin cell CR 2025) in an Ar-filled glove box. Metal lithium was used as counter and reference electrodes, Celgard 2300 as separators. The electrolyte solution was 1 M $LiPF_6$/ethylene carbonate (EC)/ dimethyl carbonate (DMC)/ethylmethyl carbonate (EMC) (1:1:1 by volume). The water content in the electrolyte was low than 1 ppm.

3. Results and discussion

Fig. 1 shows the TG–DSC curves of the mixture of precursor powders with a heating rate of 5 °C min^{-1} from room temperature to 830 °C in air. There are three temperature intervals where significant mass loss can be detected. The first one is the interval between room temperature and about 250 °C that corresponds to the superficial water loss due to the hygroscopic nature of the precursor complex and the crystal water in the sample. In the second region (250–620 °C), the endothermic peak observed at 530 °C is accompanied by noticeable weight loss in the TG curve. It can be considered as a result of the decomposition of the inorganic constituents of the precursor followed by crystallization of spinel $Li_4Ti_{4.95}La_{0.05}O_{12}$ phase. In the last region, the TG curve becomes flat, indicating that no phase transformation occurs, and that any further heating only makes the structure of samples more perfectly. However, it can be clearly seen an exothermic peaks in the DSC curves located at around 750 °C. This can be assigned to the
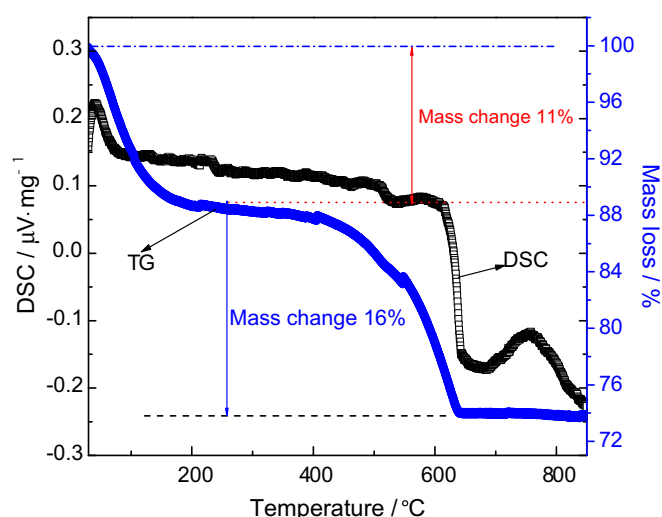

Fig. 1. TG–DSC curves of the mixture of $Li_4Ti_{4.95}La_{0.05}O_{12}$ precursor powders.

phase-change reaction (formation of $Li_4Ti_{4.95}La_{0.05}O_{12}$) and the completion of the crystallization reaction.

Fig. 2 shows the XRD patterns of the as-prepared $Li_4Ti_{5-x}La_xO_{12}$ ($0 \leq x \leq 0.2$). The diffraction patterns of all samples are similar, with all the peaks indexable in the Fd-$3m$ space group with a cubic lattice, and no impurities are observed in pure $Li_4Ti_5O_{12}$ samples. The few impurity peaks observed in the XRD patterns of Li_4Ti_{5-x}-La_xO_{12} ($0.05 \leq x \leq 0.2$) as shown in Fig. 2(b−e) indicate that La-modified $Li_4Ti_5O_{12}$ material has an impure spinel structure, and a little lanthanum element cannot substitute titanium element in the octahedron 16d site. The reason may be due to the great difference of ionic radius between La^{3+} ion (1.032 Å) [24] and Ti^{3+} ion (0.67 Å [24]). The impurity can be identified as $Li_{3x}La_{2/3-x}TiO_3$ (LLTO) according to the XRD patterns [25]. Hence, $Li_4Ti_{5-x}La_xO_{12}$ material may be a LLTO−LTO solid solution. It has been reported that LLTO exhibits a high conductivity, which can arrive at 10^{-3} s cm^{-1} at room temperature for $x = 0.1$ [26,27]. $Li_4Ti_{5-x}La_xO_{12}$ (LLTO−LTO) may have a high conductivity due to the high conductivity of LLTO. Hence, it can be expected that $Li_4Ti_{5-x}La_xO_{12}$ has a good electrochemical performance. However, the peaks of the $Li_4Ti_5O_{12}$ shift to lower diffraction angles after La modifying, indicating the lattice parameters increase after La modifying. However, the positions of the diffraction peaks of $Li_4Ti_{5-x}La_xO_{12}$ ($0.05 \leq x \leq 0.2$) almost are fixed when x values exceed 0.05. The

only difference is the intensity of the diffraction peaks for the impurity (LLTO) increases with increasing of the modified La contents. This indicates that only little La^{3+} can enter the crystal lattice of $Li_4Ti_5O_{12}$, and the modifying of lanthanum element makes the crystal lattice expand to a certain extent because the radius of La^{3+} ion is greater than that of Ti^{3+} ion. The expansile channels reduce the block for the diffusion of Li^+, and then improve the electrochemical performance of the material.

Raman spectra of $Li_4Ti_{5-x}La_xO_{12}$ ($0 \leq x \leq 0.2$) are shown in Fig. 3. The typical Raman scattering features of the pristine $Li_4Ti_5O_{12}$ are well-evidenced in all samples. Each spectrum shows five main Raman bands peaked at about 257, 348, 423, 674, and 748 cm^{-1} representing the features of the spinel structure ($A_{1g} + E_g + 3F_{2u}$) [28]. The only difference is that the intensities of Raman signals for modified samples are higher than that for the pristine compound. The most intense Raman signal at 673 cm^{-1} can be assigned to Ti−O stretches in "TiO$_6$" octahedral. The middle frequency bands at 348 and 423 cm^{-1} can be assigned to the stretching vibrations of the Li−O bonds in LiO$_4$ and LiO$_6$ polyhedra, respectively [29]. This observation demonstrates the modification cannot change the basic spinel structure of $Li_4Ti_5O_{12}$.

Typical scanning electron microscope (SEM) images of the as-prepared $Li_4Ti_{5-x}La_xO_{12}$ ($x = 0, 0.05, 0.1$) are shown in Fig. 4. It is apparent that the morphologies of three samples are similar. All material is well crystallized with a uniform and narrow size distribution in the range of 1−2 μm.

Fig. 5 presents typical steady-state cyclic voltammograms (CVs) of $Li_4Ti_{5-x}La_xO_{12}$ ($0 \leq x \leq 0.2$) electrodes obtained at a scan rate of 0.2 mV s^{-1}. The narrow oxidation peaks at about 1.7 V (anodic delithiation) and the reduction peak at 1.5 V (cathodic lithiation) can be attributed solely to the successive oxidation/reduction reactions of the Ti^{3+}/Ti^{4+} couple in the cubic structure, compensated by lithium deinsertion−insertion. The voltage difference of the $Li_4Ti_{5-x}La_xO_{12}$ ($0 \leq x \leq 0.2$) electrodes between oxidation and reduction peaks is listed in Fig. 5. ΔE ($\varphi_a - \varphi_c$) is 244 mV for the pristine electrode, obviously much larger than those for the La-modified electrodes. $Li_4Ti_{5-x}La_xO_{12}$ ($x = 0.05$) sample shows the lowest potential interval between anodic and cathodic peak (207 mV). The potential interval can be determined by the potential polarization of the active material during charge and discharge process. Hence, the low potential interval demonstrates that the lithium insertion into the La-modified $Li_4Ti_5O_{12}$ composite behaves more likely as a Nernst system [30]. All these analyses show that the improved dynamic behaviors can be attributed to the La
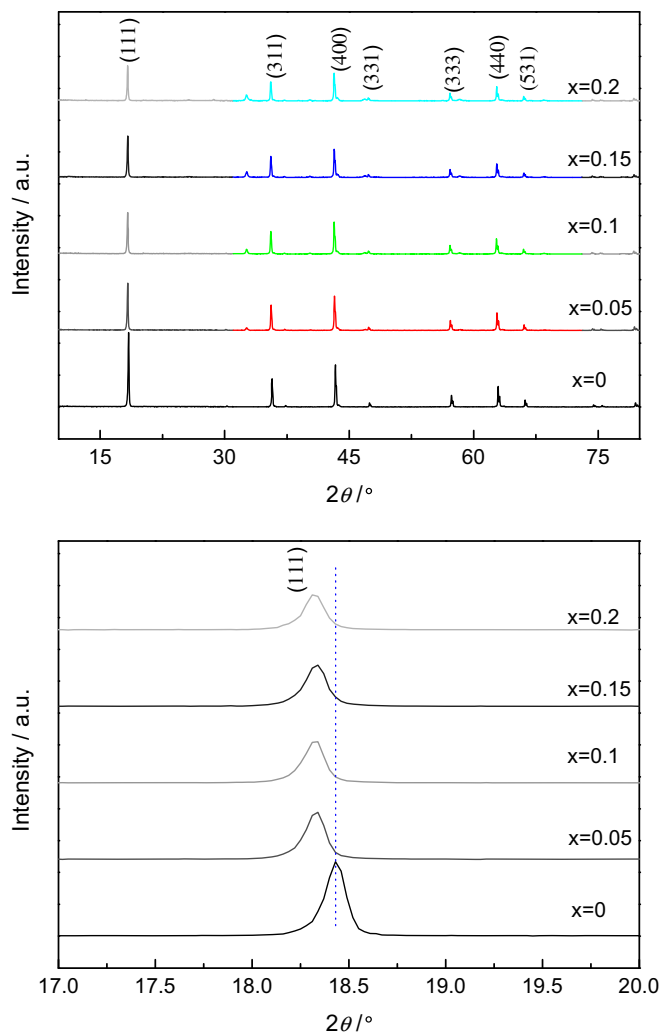

Fig. 2. XRD pattern of as-prepared $Li_4Ti_{5-x}La_xO_{12}$ (a) $x = 0$; (b) $x = 0.05$; (c) $x = 0.1$; (d) $x = 0.15$; (e) $x = 0.2$.
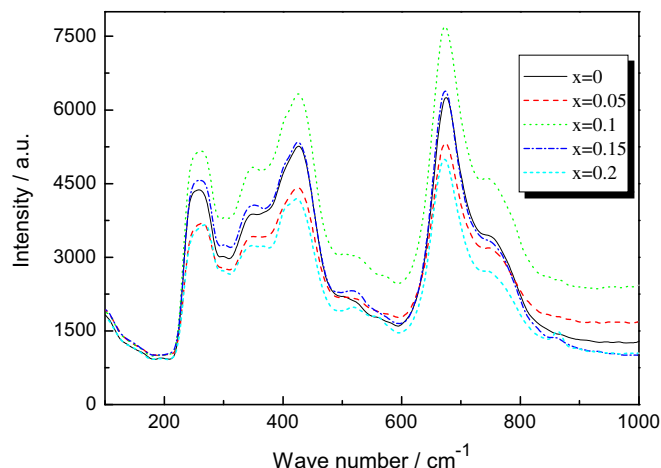

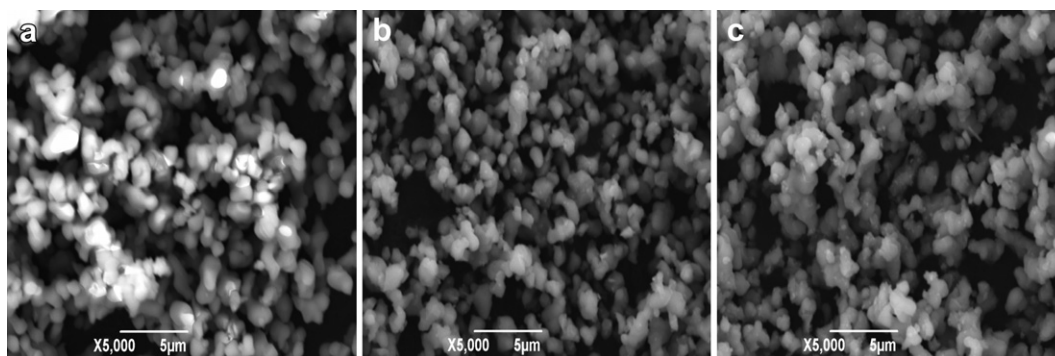**Fig. 3.** Raman spectra of as-prepared $Li_4Ti_{5-x}La_xO_{12}$ ($x = 0, 0.05, 0.1, 0.15, 0.2$) samples.

Fig. 4. SEM images of $Li_4Ti_{5-x}La_xO_{12}$ prepared by the solid-state method (a) $x = 0$, (b) $x = 0.05$ and (c) $x = 0.1$.

modifying. Based on the results, it can be concluded that the reversibility and electrochemical performance of La-modified $Li_4Ti_5O_{12}$ are significantly improved.

Electrochemical impedance spectroscopy (EIS) was performed on the fresh coin batteries, and the corresponding Nyquist plots of the spectra were presented in Fig. 6a. Fig. 6b shows the equivalent circuit used to fit the EIS. All spectra have a depressed semicircle in high frequency region and an inclined line in low frequency region. The sloping line in the low frequency represents lithium diffusion resistance within the anode indicating the Warburg impedance of long-range Li-ion diffusion. The capacitive loop is caused by charge transfer resistance (R_{ct}) [31,32]. The intercept impedance on the real axis corresponds to the solution resistance, and the depressed semicircles at high frequency are reflective of SEI film [33]. From Fig. 6, the charge transfer resistance of $Li_4Ti_{4.95}La_{0.05}O_{12}$ (551.1 Ω) and $Li_4Ti_{4.9}La_{0.1}O_{12}$ (489.5 Ω) is much smaller than that of $Li_4Ti_5O_{12}$ (755.9 Ω). It can be confirmed that the decrease of charge transfer resistance is beneficial to the kinetic behaviors during charge/discharge process. This indicates that La modifying in the $Li_4Ti_5O_{12}$ is favorable to improve the conductivity, and then lead to the improvement of rate performance. As mentioned above, the $Li_4Ti_{5-x}La_xO_{12}$ ($0.05 \leq x \leq 0.2$) may be a LLTO−LTO solid solution. It can be concluded that La modifying in the $Li_4Ti_5O_{12}$ is favorable to improve the conductivity due to the formation of LLTO. In addition, the increased slope in the low frequency end for the $Li_4Ti_{4.95}La_{0.05}O_{12}$ sample indicates that $Li_4Ti_{4.95}La_{0.05}O_{12}$ has the highest Li migration among all samples. According to the electrochemical results mentioned above, clearly, $Li_4Ti_{4.95}La_{0.05}O_{12}$ has the best kinetic performance among all samples.

The EIS can be used to calculate the lithium diffusion coefficient (D_{Li}) using the following equation [34,35]

$$Z_{re} = R_{ct} + R_s + \sigma\omega^{-\frac{1}{2}} \tag{1}$$

$$D_{Li} = \frac{R^2T^2}{2A^2n^4F^4C_{Li}^2\sigma^2} \tag{2}$$

where the meanings of T is the absolute temperature, R the gas constant, n the number of electrons per molecule during oxidization, A the surface area, F the Faraday's constant, C_{Li} the concentration of lithium ion in solid (4.37×10^{-3} mol cm^{-3}) [36], ω the angular frequency, and σ is the Warburg factor which has a relationship with Z_{re}. The $Z_{re} - \omega^{-1/2}$ plots were presented in Fig. 7. The lithium diffusion coefficients of $Li_4Ti_{5-x}La_xO_{12}$ ($x = 0$, 0.05, 0.1) are calculated to be 7.79×10^{-15}, 10.98×10^{-15} and 5.27×10^{-15} cm^2 s^{-1}, respectively. It can be found that $Li_4Ti_{4.95}La_{0.05}O_{12}$ has the highest lithium diffusion coefficient among three samples. The lowest lithium diffusion coefficient of $Li_4Ti_{4.9}La_{0.1}O_{12}$ may be due to the much impurity (See Fig. 2), and then block the migration of lithium ions. Therefore, $Li_4Ti_{4.95}La_{0.05}O_{12}$ sample with uniform morphology, narrow size distribution, little agglomerations, high electronic conductivity and large lithium diffusion coefficient would exhibit much better electrochemical performance than the pure $Li_4Ti_5O_{12}$.

The cycling performance and initial charge−discharge curves of the annealed $Li_4Ti_{5-x}La_xO_{12}$ ($0 \leq x \leq 0.2$) samples at 0.5 C charge−discharge rate are shown in Fig. 8. Each sample shows a flat
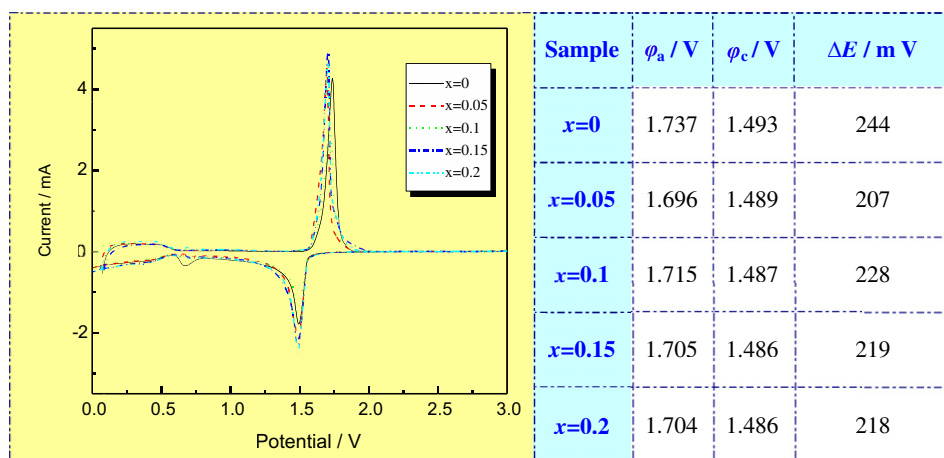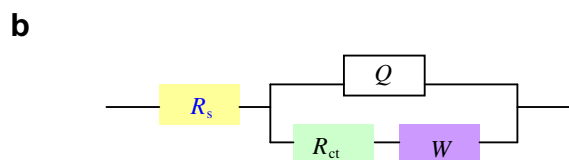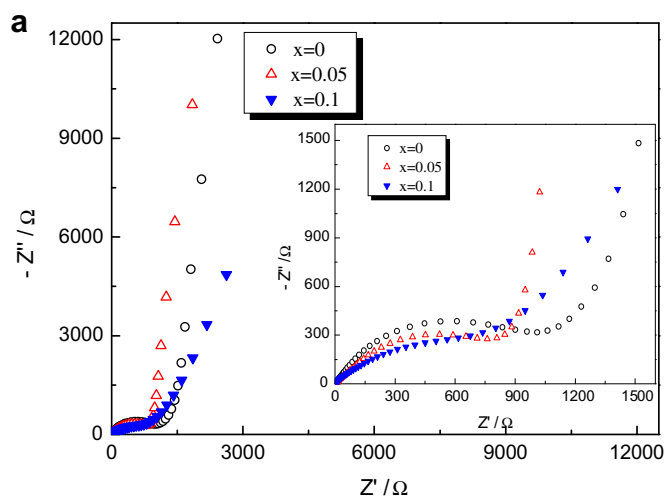

Sample	φ_a / V	φ_c / V	ΔE / mV
x=0	1.737	1.493	244
x=0.05	1.696	1.489	207
x=0.1	1.715	1.487	228
x=0.15	1.705	1.486	219
x=0.2	1.704	1.486	218

Fig. 5. Cyclic voltammerty (CV) and values of the CV peaks for $Li_4Ti_{5-x}La_xO_{12}$ ($0 \leq x \leq 0.2$)/Li cell between 0 V and 3 V.

a

b

Fig. 6. (a) Nyquist plots for $Li_4Ti_{5-x}La_xO_{12}$ ($x = 0, 0.05, 0.1$) electrodes; (b) the equivalent circuit used to fit the EIS. Inset is the enlarged Nyquist plots.

plateaus around 1.5–1.6 V (versus Li/Li$^+$), which correspond to the reversible phase transition between $Li_4Ti_5O_{12}$ and $Li_7Ti_5O_{12}$. Obviously, $Li_4Ti_5O_{12}$ is able to host more Li when cycled to a lower potential. The $Li_4Ti_5O_{12}$ electrode shows a slightly higher initial capacity than that of La-modified $Li_4Ti_5O_{12}$ due to the highest amount of titanium ions in $Li_4Ti_5O_{12}$ spinel phase. A large irreversible capacity for all electrodes in the second cycle is mainly attributed to some side reactions for solid electrolyte interface (SEI) formation and lithium adsorption in the carbon black [37,38]. In addition, some lithium ions occupied 48f sites cannot be extracted out electrochemically, and this can also lead the irreversible capacity [15,39]. $Li_4Ti_{4.95}La_{0.05}O_{12}$ shows the highest discharge capacity among all samples between 0.0 and 2.5 V at 0.5 C charge–discharge rate. Rate capabilities for $Li_4Ti_{5-x}La_xO_{12}$
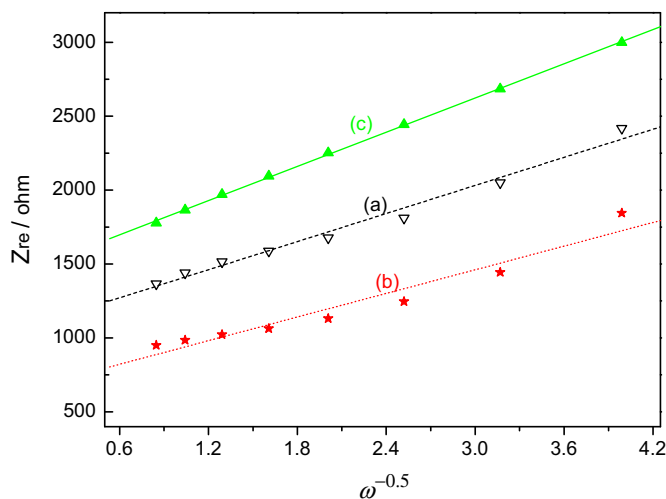
Fig. 7. Graph of Z_{re} plotted against $\omega^{-1/2}$ at low frequency region for $Li_4Ti_{5-x}La_xO_{12}$ electrodes (a) $x = 0$, (b) $x = 0.05$ and (c) $x = 0.1$.
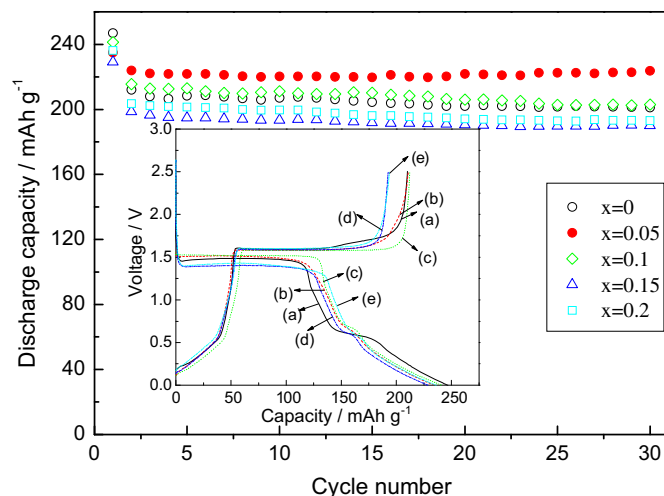
Fig. 8. Cycling performance of $Li_4Ti_{5-x}La_xO_{12}$ ($x = 0, 0.05, 0.1, 0.15, 0.2$) at 0.5 C charge–discharge rate. Inset is the initial charge–discharge curves.

($0 \leq x \leq 0.2$) are shown in Fig. 9. $Li_4Ti_{4.95}La_{0.05}O_{12}$ reaches a reversible capacity of 206.9 mAh g^{-1} at 1 C charge–discharge rate after 100 cycles, which keeps 97% of its discharge capacity at the second cycle (213.6 mAh g^{-1}) and 69% of the theoretical capacity (298 mAh g^{-1}). $Li_4Ti_{5-x}La_xO_{12}$ ($0.1 \leq x \leq 0.2$) materials have a relative lower discharge capacity at low charge–discharge rate. Based on our previous studies [16,19], it is known that almost all the electrochemical energy comes from the reversible redox reactions between trivalent titanium ion (Ti^{3+}) and tetravalent titanium ion (Ti^{4+}). Hence, the increase of the modified La can decrease the amount of active titanium ions, and then reduce the discharge capacity. However, better electrochemical performance for La-modified $Li_4Ti_5O_{12}$ materials was found with increasing of charge–discharge rate. At 3 C rate, the reversible capacities for $Li_4Ti_{4.95}La_{0.05}O_{12}$ and $Li_4Ti_5O_{12}$ are 197.9 and 187.7 mAh g^{-1} after 100 cycles, respectively. $Li_4Ti_{5-x}La_xO_{12}$ ($0.05 \leq x \leq 0.15$) materials have higher reversible capacities than that of pristine $Li_4Ti_5O_{12}$ after 100 cycles. At 5 C rate, the reversible capacities of $Li_4Ti_{5-x}La_xO_{12}$ ($x = 0, 0.05, 0.1, 0.15, 0.2$) are 175.7, 181.1, 176.4, 180.6 and 179 mAh g^{-1} after 200 cycles, respectively. The results indicate that rate cyclic performance of $Li_4Ti_5O_{12}$ at room temperature can be markedly improved by La modifying. Hence, it can be concluded that the structure of La-modified $Li_4Ti_5O_{12}$ is very stable for lithium ions insertion and extraction during high rate cycling. These may be explained by the facts that: (1) smaller particles can provide more interfacial area for contact within the liquid electrolyte and hence can be beneficial for Li ion batteries as a result of providing short diffusion length; (2) the relatively higher conductivity and lithium diffusion coefficient would help to release the stresses generated by the repetitive Li$^+$ intercalation, and then reduce the electrochemical polarization during high rate charge–discharge. Based on the above results, it can be confirmed that modifying with La^{3+} can improve the rate-capacity and cyclic reversibility of $Li_4Ti_5O_{12}$. However, the contents of modified La have strong impact on the rate capability of $Li_4Ti_5O_{12}$ electrode. Hence, it is important that a proper La modifying level should be optimized to achieve a good cell performance. From the overall performance point of view, sample $Li_4Ti_{4.95}La_{0.05}O_{12}$ shows the best electrochemical performance among all samples. Therefore, the high energy density (discharge to 0 V) together with good high rate cycling performance of the prepared $Li_4Ti_{4.95}La_{0.05}O_{12}$ material by the simple solid-state method make it a promising alternative to next generation lithium-ion batteries.
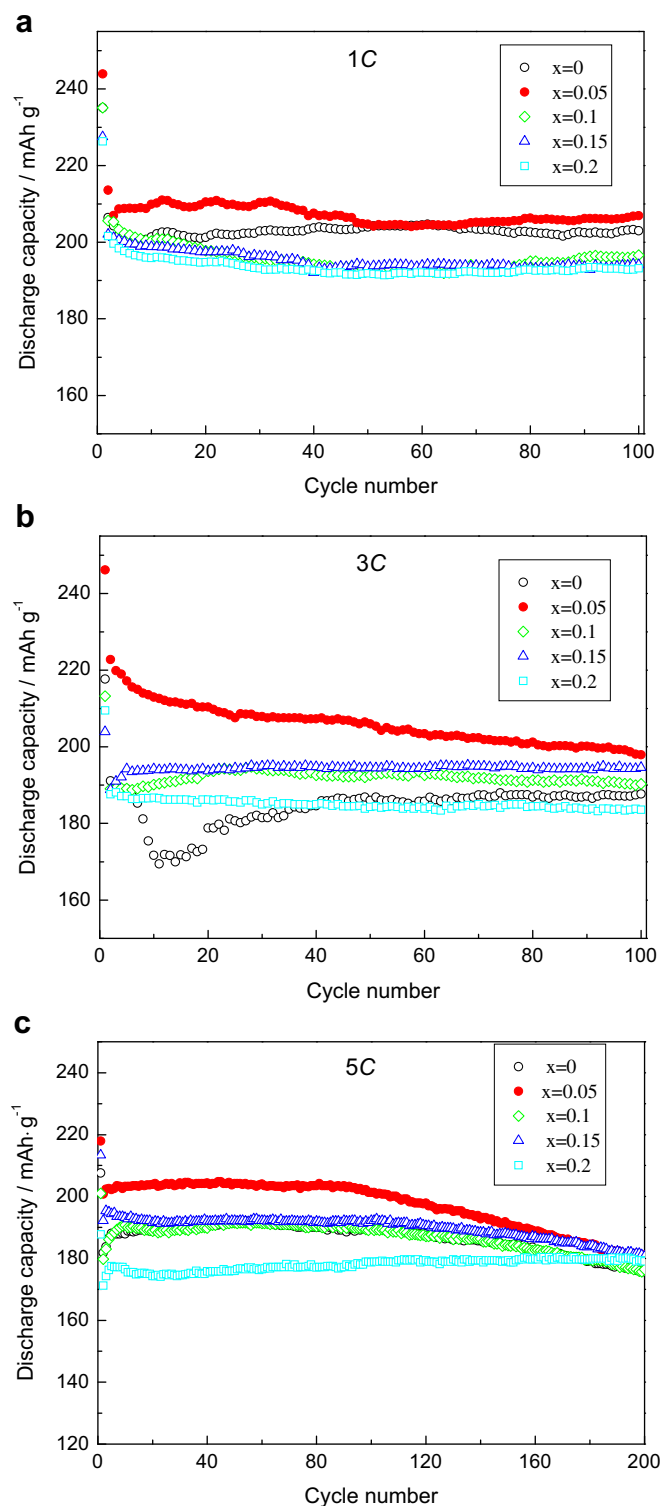
Fig. 9. Capacity retention upon cycling for $Li_4Ti_{5-x}La_xO_{12}$ ($0 \leq x \leq 0.2$) at different charge−discharge rates between 2.5 and 0.0 V (a) 1 C, (b) 3 C and (d) 5 C.

with an average particle size of approximately 1−2 μm. La modifying enlarges the Li^+ ion transport channel, resulting in a significantly great capacity and cycling stability of $Li_4Ti_5O_{12}$ at high charge−discharge rate. $Li_4Ti_{4.95}La_{0.05}O_{12}$ electrode exhibits the highest conductivity and lithium diffusion coefficient during Li^+ extraction among all samples. The resulting $Li_4Ti_{4.95}La_{0.05}O_{12}$ sample demonstrates remarkable rate capability in that it delivers a reversible capacity of 200.8 mAh g^{-1} at the second cycle, and still retains 90.2% of the capacity (vs. 2nd cycle) at 5 C charge−discharge rate after 200 cycles. The $Li_4Ti_{4.95}La_{0.05}O_{12}$ anode described in the present work is capable of large-scale applications, such as electric vehicles and plug-in hybrid electric vehicles, requiring fast charge, long life, high power and a wide operating voltage range, and also for stationary energy storage systems emphasizing cycle life, calendar lifespan and high safety.

Acknowledgments

References

[1] J. Hassoun, P. Reale, S. Panero, B. Scrosati, M. Wachtler, M. Fleischhammer, M. Kasper, M.W. -Mehrens, Electrochim. Acta 55 (2010) 4194−4200.
[2] N. Ohta, K. Takada, L. Zhang, R. Ma, M. Osada, T. Sasaki, Adv. Mater. 18 (2006) 2226−2229.
[3] S.S. Zhang, J. Power Sources 161 (2006) 1385−1391.
[4] T.-F. Yi, L.-J. Jiang, J. Shu, C.-B. Yue, R.-S. Zhu, H.-B. Qiao, J. Phys. Chem. Solids 71 (2010) 1236−1242.
[5] B. Zhang, H. Du, B. Li, F. Kang, Electrochem. Solid-State Lett. 13 (2010) A36−A38.
[6] C.H. Chen, J.T. Vaughey, A.N. Jansen, D.W. Dees, A.J. Kahaian, T. Goacher, M.M. Thackeray, J. Electrochem. Soc. 148 (2001) A102−A104.
[7] A.D. Robertson, L. Trevino, H. Tukamoto, J.T.S. Irvine, J. Power Sources 81−82 (1999) 352−357.
[8] Z. Wang, G. Chen, J. Xu, Z. Lv, W. Yang, J. Phys. Chem. Solids 72 (2011) 773−778.
[9] Y.-J. Hao, Q.-Y. Lai, J.-Z. Lu, X.-Y. Ji, Ionics 13 (2007) 369−373.
[10] J. Gao, C. Jiang, C. Wan, J. Electrochem. Soc. 157 (2010) K39−K42.
[11] J. Gao, J. Ying, C. Jiang, C. Wan, Ionics 15 (2009) 597−601.
[12] S. Huang, Z. Wen, X. Zhu, Z. Lin, J. Power Sources 165 (2007) 408−412.
[13] X. Li, M. Qu, Z. Yu, J. Alloys Compd. 487 (2009) L12−L17.
[14] Z. Zhong, Electrochem. Solid-State Lett. 10 (2007) A267−A269.
[15] Y.-R. Jhan, C.-Y. Lin, J.-G. Duh, Mater. Lett. 65 (2011) 2502−2505.
[16] T.-F. Yi, J. Shu, Y.-R. Zhu, X.-D. Zhu, C.-B. Yue, A.-N. Zhou, R.-S. Zhu, Electrochim. Acta 54 (2009) 7464−7470.
[17] Z. Yu, X. Zhang, G. Yang, J. Liu, J. Wang, R. Wang, J. Zhang, Electrochim. Acta 56 (2011) 8611−8617.
[18] B. Tian, H. Xiang, L. Zhang, Z. Li, H. Wang, Electrochim. Acta 55 (2010) 5453−5458.
[19] T.-F. Yi, Yi Xie, J. Shu, Z. Wang, C.-B. Yue, R.-S. Zhu, H.-B. Qiao, J. Electrochem. Soc. 158 (2011) A266−A274.
[20] J. Wolfenstine, J.L. Allen, J. Power Sources 180 (2008) 582−585.
[21] S. Huang, Z. Wen, Z. Gu, X. Zhu, Electrochim. Acta 50 (2005) 4057−4062.
[22] Y. Qi, Y. Huang, Di. Jia, S.-J. Bao, Z.P. Guo, Electrochim. Acta 54 (2009) 4772−4776.
[23] M.-S. Wu, P.-C. Julia Chiang, J.-C. Lin, Y.-S. Jan, Electrochim. Acta 49 (2004) 1803−1812.
[24] R.D. Shannon, Acta Crystallogr. A32 (1976) 751−767.
[25] L. Sun, N. Karanjgaokar, K. Sun, I. Chasiotis, W.C. Carter, S. Dillon, J. Power Sources 196 (2011) 6507−6511.
[26] H. Kawai, J. Kuwano, J. Electrochem. Soc. 141 (1994) L78−L79.
[27] O. Bohnke, C. Bohnke, J.L. Fourquet, Solid State Ionics 91 (1996) 21−31.
[28] L. Aldon, P. Kubiak, M. Womes, J.C. Jumas, J. Olivier-Fourcade, J.L. Tirado, J.I. Corredor, C. Perez Vicente, Chem. Mater. 16 (2004) 5721−5725.
[29] R. Baddour-Hadjean, J.-P. Pereira-Ramos, Chem. Rev. 110 (2010) 1278−1319.
[30] L. Xiao, Y. Zhao, Y. Yang, Y. Cao, X. Ai, H. Yang, Electrochim. Acta 54 (2008) 545−550.
[31] G.T.-K. Fey, C.Z. Lu, T.P. Kumar, J. Power Sources 115 (2003) 332−345.

4. Conclusions

We introduce a synthesis of micro-sized La-modified $Li_4Ti_5O_{12}$ anode material and a new approach to enhance the rate performance of $Li_4Ti_5O_{12}$ anode material by La modifying. La modifying results in the formation of $Li_{3x}La_{2/3-x}TiO_3$-$Li_4Ti_5O_{12}$ solid solution

[32] Y. Wang, H. Liu, K. Wang, H. Eiji, Y. Wang, H. Zhou, J. Mater. Chem. 19 (2009) 6789–6795.
[33] L. Yang, L. Gao, J. Alloys Compd. 485 (2009) 93–97.
[34] G.Q. Liu, H.T. Kuo, R.S. Liu, C.H. Shen, D.S. Shy, X.K. Xing, J.M. Chen, J. Alloys Compd. 496 (2010) 512–516.
[35] Q. Cao, H.P. Zhang, G.J. Wang, Q. Xia, Y.P. Wu, H.Q. Wu, Electrochem. Commun. 9 (2007) 1228–1232.
[36] S.-L. Chou, J.-Z. Wang, H.-K. Liu, S.-X. Dou, J. Phys. Chem. C 115 (2011) 16220–16227.
[37] W.J.H. Borghols, M. Wagemaker, U. Lafont, E.M. Kelder, F.M. Mulder, J. Am. Chem. Soc. 131 (2009) 17786–17792.
[38] X.L. Yao, S. Xie, H.Q. Nian, C.H. Chen, J. Alloys Compd. 465 (2008) 375–379.
[39] J. Shu, J. Solid State Electrochem. 13 (2009) 1535–1539.